

Inelastic mean-free paths and surface excitation parameters by absolute reflection electron-energy loss measurements

T. Nagatomi^{1,*} and K. Goto²¹*Department of Material and Life Science, Division of Advanced Science and Biotechnology, Graduate School of Engineering, Osaka University, Suita, Osaka 565-0871, Japan*²*National Institute of Advanced Industrial Science and Technology (AIST) Chubu, Moriyama-ku, Nagoya, Aichi 463-8560, Japan*

(Received 18 August 2006; revised manuscript received 19 December 2006; published 18 June 2007)

An analytical approach is proposed for simultaneously determining the inelastic mean-free path (IMFP), the surface excitation parameter (SEP), and the differential SEP (DSEP) in absolute units from an absolute reflection electron energy loss spectroscopy (REELS) spectrum under the assumption that the normalized differential inelastic mean-free path for bulk excitations and the elastic scattering cross section are known. This approach was applied to an analysis of REELS spectra for Ni, and the IMFP, SEP, and DSEP in Ni for 300–3000 eV electrons were determined. The resulting IMFPs showed good agreement with those calculated using the TPP-2M predictive equations and with those calculated from optical data. The deduced DSEPs show a reasonable agreement with those theoretically predicted. The obtained SEPs were compared with those calculated using several predictive equations. The present SEP results agreed well with the Chen formula with a material parameter proposed for Ni. The present approach has high potential for the experimental determination of IMFPs, SEPs, and DSEPs in absolute units.

DOI: [10.1103/PhysRevB.75.235424](https://doi.org/10.1103/PhysRevB.75.235424)

PACS number(s): 82.80.Pv, 79.20.–m, 79.20.Uv, 73.20.Mf

I. INTRODUCTION

Quantitative information on the inelastic interaction of medium-energy electrons with solids is of importance for the accurate quantification of experimental spectra obtained by Auger electron spectroscopy, x-ray photoelectron spectroscopy, and reflection electron energy loss spectroscopy (REELS). Signal electrons used in these surface chemical analysis techniques undergo multiple elastic and inelastic-scattering events during transport in solids. Electrons losing their kinetic energy through various types of inelastic scattering processes are detected at energies far from those of corresponding peaks in a measured spectrum. One of the most important factors for the accurate quantification of measured spectra is the inelastic mean-free path (IMFP) describing the decay of the peak intensity by inelastic scattering occurring in the bulk. To improve the accuracy of the quantification, theoretical and experimental determinations of the IMFP have been intensively studied.^{1–9} Recent studies revealed that an energy-loss process due to excitation modes localized in the near-surface region, i.e., surface excitations, plays an important role in inelastic interaction, resulting in a significant decay of the intensity of signal electrons.¹⁰ These findings suggest that a correction for the decay of the peak intensity by surface excitations might be required for accurate quantification, in addition to that for bulk excitations described by the IMFP.

With respect to the IMFP, one of the most widely used values is that calculated using the TPP-2M predictive equations.^{1–7} In order to experimentally evaluate the IMFPs, elastic peak electron spectroscopy (EPES) has been intensively studied.^{8,9} In most EPES studies dealing with the experimental determination of the IMFP, a reference material was used, the IMFP of which should be known, indicating that the IMFP obtained by the EPES analysis strongly depends on the selection of the material and the value of the

IMFP used as the reference in the analysis.^{11–13} In addition, since a recent study revealed that surface excitations cause a decay of the elastic peak intensity of 20%–70% in addition to the decay due to bulk excitations in the EPES analysis,¹⁰ several EPES studies have been performed by correcting the decay of the elastic peak intensity due to surface excitations using predictive equations for a surface excitation parameter (SEP).^{14,15} In such studies, the decay of the elastic peak intensity due to both bulk and surface excitations are taken into account, and the resultant IMFP depends on the predictive equation for the SEP as well as on the reference material and IMFP.^{14,15} Thus a SEP is also one of the most important factors for accurate quantification.

Studies on surface excitations for medium-energy electrons have been intensively performed both experimentally and theoretically.^{16–21} For the experimental determination of the SEP, two analytical methods have been applied in those studies. One is the EPES analysis^{10,14,15,22,23} and the other is the REELS analysis.^{24–30} The EPES analysis requires the same reference material as that applied for the determination of the IMFP, indicating that the SEP determined by the EPES analysis depends on the selection of the reference material.^{15,22,23} EPES analysis in absolute units does not require a reference material.¹⁰ The REELS analysis also does not require the reference material.^{24–30} However, in all the EPES and REELS analyses performed for determining the SEP, the IMFP is taken from the literature and the derived SEP depends on the IMFP used in the analysis.

From a physical point of view, one of the most promising approaches is the simultaneous determination of the IMFP and SEP.³¹ In the present study, therefore, an analytical approach for simultaneously determining both the IMFP and SEP from absolute REELS spectra is proposed. The present approach is based on the Landau theory³² describing the transport of charged particles in solids. A response function of a REELS spectrum is self-consistently deconvoluted into

components relevant to electrons participating in m -fold bulk and l -fold surface excitation events, and the IMFP, SEP, and differential SEP (DSEP) are determined in absolute units.

II. EXPERIMENT

The REELS spectra analyzed in the present study were those measured in absolute units using the cylindrical mirror analyzer (CMA) developed by one of the authors.³³ The CMA was equipped with a Faraday cup as a detector, which enables the absolute electron current to be measured. The sample was polycrystalline Ni, the surface of which was sputter cleaned with 250–3000 eV Ar⁺ ions. The root-mean-square (rms) roughness of the sample surface was confirmed to be 3–5 nm within a region of 10 μm^2 by means of atomic force microscopy. The primary electron energies were 300–3000 eV, the beam current was 1 μA for all measurements, and the beam was incident normally on the sample. The analyzer detection and acceptance angles were $42.3^\circ \pm 6^\circ$. The energy resolution of the system was 0.25%. The base pressure of the apparatus was 2×10^{-8} Pa. Details of the experimental setup are described elsewhere.¹⁰

III. THEORY

The deconvolution procedure in the present study is based on the Landau theory,³² and a similar procedure has been intensively studied.^{24–27,34–36} Here, formulation and assumptions made in the present study are outlined below. The original Landau equation describes energy losses of electrons during transport in solids under the assumption that changes of the electron direction of motion can be neglected.³² The Landau theory can be extended by taking into account the effects of angular deflections of moving electrons by elastic scattering, and is given in Fourier space of the energy^{37–39}

$$J(s) = F(s) \sum_{m=0}^{\infty} \alpha_m [\lambda_b K_b(s)]^m, \quad (1)$$

where $J(s)$, $F(s)$, and $K_b(s)$ are Fourier transforms of the measured REELS spectrum $J(E)$, the energy distribution of primary electrons $F(E)$, and the differential inverse mean-free path (DIMFP) for bulk excitations $K(\Delta E)$, respectively. s is the Fourier parameter conjugate to the energy E , and ΔE is the energy loss. m is the number of bulk excitation events undergone by signal electrons during transport in the solid. α_m is the probability that primary electrons experience m -fold bulk excitation events in the solid before being emitted from the surface. λ_b is the IMFP, which satisfies the following equation with the differential IMFP (DIMFP):

$$1 = \lambda_b \int_0^{E_0} K_b(\Delta E) d(\Delta E), \quad (2)$$

where E_0 is the primary electron energy. The extension of the Landau theory expressed by Eq. (1) is the generalization of the Landau theory in the case that the elastic and inelastic scattering are independent processes. This circumstance is well-approximated to be valid for medium-energy electrons,

since the inelastic transport mean-free path is at least one order of magnitude larger than the elastic one and the energy transfer in an elastic collision is usually negligibly small, as discussed in detail in the literature.^{35,40}

By assuming that surface excitations can be described on the basis of the Poisson stochastic process occurring when signal electrons cross the surface,^{41–43} the Landau theory expressed by Eq. (1) can be further extended to include energy-loss processes due to surface excitations, and is rewritten^{34–36}

$$J(s) = F(s) \sum_{m=0}^{\infty} \alpha_m [\lambda_b K_b(s)]^m \sum_{l_{\text{in}}=0}^{\infty} P_s^{\text{in}, l_{\text{in}}} [K_s^{\text{in}}(s)/P_s^{\text{in}}]^{l_{\text{in}}} \times \sum_{l_{\text{out}}=0}^{\infty} P_s^{\text{out}, l_{\text{out}}} [K_s^{\text{out}}(s)/P_s^{\text{out}}]^{l_{\text{out}}}. \quad (3)$$

The Σ terms with respect to the integration over l_{in} and l_{out} describe energy-loss processes due to surface excitations on incoming and outgoing trajectories, respectively. l_{in} and l_{out} are the numbers of surface excitations undergone by incoming and outgoing electrons. P_s^{in} and P_s^{out} are the SEPs for incoming and outgoing electrons. $K_s^{\text{in}}(s)$ and $K_s^{\text{out}}(s)$ are the Fourier transforms of the differential SEPs (DSEPs) for incoming and outgoing electrons, $K_s^{\text{in}}(\Delta E)$ and $K_s^{\text{out}}(\Delta E)$. The SEP and DSEP for incoming and escaping electrons satisfy the following relations, similarly to the IMFP and DIMFP for bulk excitations.

$$1 = (P_s^{\text{in}})^{-1} \int_0^{\infty} K_s^{\text{in}}(\Delta E) d(\Delta E), \quad (4)$$

$$1 = (P_s^{\text{out}})^{-1} \int_0^{\infty} K_s^{\text{out}}(\Delta E) d(\Delta E), \quad (5)$$

$P_s^{\text{in}, l_{\text{in}}}$ and $P_s^{\text{out}, l_{\text{out}}}$ are the probabilities that electrons participate in l_{in} - and l_{out} -fold surface excitations, and are given by

$$P_s^{\text{in}, l_{\text{in}}} = \frac{(P_s^{\text{in}})^{l_{\text{in}}}}{l_{\text{in}}!} \exp(-P_s^{\text{in}}) \quad (6)$$

$$P_s^{\text{out}, l_{\text{out}}} = \frac{(P_s^{\text{out}})^{l_{\text{out}}}}{l_{\text{out}}!} \exp(-P_s^{\text{out}}). \quad (7)$$

Here, Eq. (3) is valid when the coupling between surface and bulk losses is uncorrelated and interference effects between the incoming and outgoing part of the trajectory are neglected. The former condition is satisfied for medium-energy electrons since the thickness of the surface scattering layer is smaller than or of the order of the elastic mean-free path.^{25,35} The latter circumstance is also satisfied since interference effects between the incoming and outgoing part of the trajectory cancel out to a high degree when a large number of trajectories are taken into account.³⁵

As discussed in Ref. 44, the shape of the DSEP, i.e., the normalized DSEP, is independent of the surface crossing direction. Under such a condition, the dependence of the SEP and DSEP on the moving directions of incoming and escaping electrons with respect to the surface normal, θ_{in} and θ_{out} , respectively, can be approximated to be cosine dependence,

and provides the following relations of SEP and DSEP between the incoming and outgoing trajectories:

$$K_s^{\text{out}}(\Delta E) = \Theta(\theta_{\text{in}}, \theta_{\text{out}}) K_s^{\text{in}}(\Delta E) \quad (8)$$

$$P_s^{\text{out}} = \Theta(\theta_{\text{in}}, \theta_{\text{out}}) P_s^{\text{in}} \quad (9)$$

$$\Theta(\theta_{\text{in}}, \theta_{\text{out}}) = \cos \theta_{\text{in}} / \cos \theta_{\text{out}}. \quad (10)$$

Using Eqs. (8)–(10), Eq. (3) can be rewritten as

$$J(s) = F(s) \sum_{m=0}^{\infty} \alpha_m [\lambda_b K_b(s)]^m \sum_{l_{\text{in}}=0}^{\infty} \sum_{l_{\text{out}}=0}^{\infty} P_s^{\text{in}, l_{\text{in}}} P_s^{\text{out}, l_{\text{out}}} \times [K_s^{\text{in}}(s)/P_s^{\text{in}}]^{(l_{\text{in}}+l_{\text{out}})}. \quad (11)$$

We can now set the total number of surface excitations l as

$$l = l_{\text{in}} + l_{\text{out}}. \quad (12)$$

Then, Eq. (11) becomes

$$J(s) = F(s) \sum_{m=0}^{\infty} \alpha_m [\lambda_b K_b(s)]^m \sum_{l=0}^{\infty} P_s^{\text{total}, l} [K_s^{\text{in}}(s)/P_s^{\text{in}}]^l, \quad (13)$$

where $P_s^{\text{total}, l}$ is given by

$$P_s^{\text{total}, l} = \sum_{l_{\text{in}}=0}^l P_s^{\text{in}, l_{\text{in}}} P_s^{\text{out}, (l-l_{\text{in}})} = \sum_{l_{\text{in}}=0}^l \frac{[\Theta(\theta_{\text{in}}, \theta_{\text{out}})]^{(l-l_{\text{in}})} (P_s^{\text{in}})^l}{l_{\text{in}}!(l-l_{\text{in}})!} \times \exp\{-[1 + \Theta(\theta_{\text{in}}, \theta_{\text{out}})] P_s^{\text{in}}\} \quad (14)$$

and describes the probability that signal electrons participate in l -fold surface excitations. Equation (13) corresponds to the expression of Eq. (48) in Ref. 35 in Fourier space.

The Landau theory can be written in real space as

$$J(E) = \int_{-\infty}^{\infty} F(E_0) R(E_0 - E) dE_0, \quad (15)$$

where $E_0 - E = \Delta E$ is the energy loss. $R(\Delta E)$ is the response function describing electron transport, i.e., all elastic- and inelastic-scattering processes, in solids and satisfies $R(\Delta E) = 0$ for $E_0 - E = \Delta E < 0$. Then, Eqs. (13) and (15) provide

$$R(\Delta E) = FT^{-1} [J(s)/F(s)] = FT^{-1} \left\{ \sum_{m=0}^{\infty} \alpha_m [\lambda_b K_b(s)]^m \sum_{l=0}^{\infty} P_s^{\text{total}, l} [K_s^{\text{in}}(s)/P_s^{\text{in}}]^l \right\}, \quad (16)$$

where FT^{-1} represents the inverse Fourier transform. By expressing the right-hand side of Eq. (16) in the real (energy) space, the following equation is obtained:

$$R(\Delta E) = \left\{ \sum_{m=0}^{\infty} \alpha_m [\lambda_b K_b(\Delta E)]^m \otimes^m [\lambda_b K_b(\Delta E)] \right\} \otimes \left\{ \sum_{l=0}^{\infty} P_s^{\text{total}, l} [K_s^{\text{in}}(s)/P_s^{\text{in}}]^l \otimes^l [K_s^{\text{in}}(s)/P_s^{\text{in}}] \right\}, \quad (17)$$

where \otimes denotes convolution, and \otimes^m and \otimes^l represent

m - and l -fold self-convolutions. Since the IMFP and DIMFP and SEP and DSEP satisfy Eqs. (2) and (4), $[\lambda_b K_b(\Delta E)] \otimes^m [\lambda_b K_b(\Delta E)]$ and $[K_s^{\text{in}}(s)/P_s^{\text{in}}] \otimes^l [K_s^{\text{in}}(s)/P_s^{\text{in}}]$ in Eq. (17) represent the normalized energy-loss distributions for m -fold bulk- and l -fold surface-excitation events, respectively. Equation (17) means that the response function $R(\Delta E)$ can be deconvoluted into components relevant to m -fold bulk and l -fold surface excitations. α_m and $P_s^{\text{total}, l}$ are the weighting functions describing the probabilities of electrons being detected after experiencing m -fold bulk and l -fold surface excitations.

Since the energy of the measured spectrum is discrete, $R(\Delta E)$ will be a set of data, $r(n)$, where $\Delta E = n\varepsilon_e$ and ε_e is the energy interval of the spectrum.

$$R(\Delta E) = R[r(0), r(1), r(2), \dots, r(n), \dots]. \quad (18)$$

In the same manner, we can also express the self-convolutions of the normalized DIMFP and DSEP as

$$x_m(n) = [\lambda_b K_b(\Delta E)] \otimes^m [\lambda_b K_b(\Delta E)], \quad (19)$$

$$y_l(n) = [K_s^{\text{in}}(\Delta E)/P_s^{\text{in}}] \otimes^l [K_s^{\text{in}}(\Delta E)/P_s^{\text{in}}].$$

From the convolution theorem, $x_m(n)$ and $y_l(n)$ satisfy

$$x_m(n) = \sum_{i=0}^n x_{m-1}(n-i) x_1(i) \varepsilon_e, \quad (20)$$

$$y_l(n) = \sum_{i=0}^n y_{l-1}(n-i) y_1(i) \varepsilon_e, \quad (20)$$

$$x_m(0) = 1, \quad (21)$$

$$y_l(0) = 1. \quad (21)$$

Using $x_m(n)$ and $y_l(n)$, the response function expressed by Eqs. (17) and (18) can be rewritten in the form

$$r(0) = \alpha_0 P_s^{\text{total}, 0},$$

$$r(n) = \sum_{m=0}^{\infty} \alpha_m x_m(n) P_s^{\text{total}, 0} + \alpha_0 \sum_{l=1}^{\infty} P_s^{\text{total}, l} y_l(n) + \sum_{j=1}^{n-1} \left[\sum_{m=1}^{\infty} \alpha_m x_m(j) \sum_{l=1}^{\infty} P_s^{\text{total}, l} y_l(n-j) \varepsilon_e \right] \quad (n \geq 1). \quad (22)$$

In order to analytically solve Eq. (22), $y_l(n)$ given by Eq. (20) is further rewritten as below. Equation (20) gives

$$y_l(n) = y_{l-1}(n) y_1(0) \varepsilon_e + y_{l-1}(0) y_1(n) \varepsilon_e + \sum_{i=1}^{n-1} y_{l-1}(n-i) y_1(i) \varepsilon_e = y_{l-1}(n) \varepsilon_e + y_1(n) \varepsilon_e + \sum_{i=1}^{n-1} y_{l-1}(n-i) y_1(i) \varepsilon_e \quad (23)$$

and

$$y_{l-1}(n) = y_{l-2}(n)\varepsilon_e + y_1(n)\varepsilon_e + \sum_{i=1}^{n-1} y_{l-2}(n-i)y_1(i)\varepsilon_e. \quad (24)$$

Using Eqs. (23) and (24), $y_l(n)$ ($l \geq 2$) expressed by Eq. (20) is rewritten as

$$y_l(n) = \left(\varepsilon_e^{l-1} + \sum_{l'=1}^{l-1} \varepsilon_e^{l'} \right) y_1(n) + \sum_{i=1}^{n-1} \sum_{l'=1}^{l-1} y_{l'}(n-i)y_1(i)\varepsilon_e^{l'}. \quad (25)$$

Since the higher number of scattering events does not contribute to the energy-loss distribution close to the elastic

peak, the summations with respect to m and l in Eq. (22) can be restricted to a some number k . Then, $r(n)$ in Eq. (22) is rewritten as

$$r(n) = \sum_{m=0}^k \alpha_m x_m(n) P_s^{\text{total},0} + \alpha_0 P_s^{\text{total},1} y_1(n) + \alpha_0 \sum_{l=2}^k P_s^{\text{total},l} \times \left[\left(\varepsilon_e^{l-1} + \sum_{l'=1}^{l-1} \varepsilon_e^{l'} \right) y_1(n) + \sum_{i=1}^{n-1} \sum_{l'=1}^{l-1} y_{l'}(n-i)y_1(i)\varepsilon_e^{l'} \right] + \sum_{j=1}^{n-1} \left[\sum_{m=1}^k \alpha_m x_m(j) \sum_{l=1}^k P_s^{\text{total},l} y_l(n-j)\varepsilon_e \right]. \quad (26)$$

By solving Eq. (26) for $y_l(n)$, $y_1(n)$ is given by

$$y_1(n) = \left\{ r(n) - \sum_{m=0}^k \alpha_m x_m(n) P_s^{\text{total},0} - \sum_{j=1}^{n-1} \left[\sum_{m=1}^k \alpha_m x_m(j) \sum_{l=1}^k P_s^{\text{total},l} y_l(n-j)\varepsilon_e \right] - \alpha_0 \sum_{l=2}^k P_s^{\text{total},l} \sum_{i=1}^{n-1} \sum_{l'=1}^{l-1} y_{l'}(n-i)y_1(i)\varepsilon_e^{l'} \right\} / \alpha_0 \left[P_s^{\text{total},1} + \sum_{l=2}^k P_s^{\text{total},l} \left(\varepsilon_e^{l-1} + \sum_{l'=1}^{l-1} \varepsilon_e^{l'} \right) \right]. \quad (27)$$

For $n=1$, Eq. (27) is rewritten as

$$y_1(1) = \frac{r(1) - \sum_{m=0}^k \alpha_m x_m(1) P_s^{\text{total},0}}{\alpha_0 \left[P_s^{\text{total},1} + \sum_{l=2}^k P_s^{\text{total},l} \left(\varepsilon_e^{l-1} + \sum_{l'=1}^{l-1} \varepsilon_e^{l'} \right) \right]}. \quad (28)$$

Equation (28) indicates that when α_m , $x_m(n)$, $P_s^{\text{total},l}$, and $r(n)$ are evaluated, Eq. (28) gives $y_1(1)$. Then, $y_l(2)$ ($l \geq 2$) can be calculated using Eq. (20). Using calculated $y_l(2)$ ($l \geq 2$) and Eq. (27), $y_1(2)$ is obtained. In the same manner, the DSEP $y_1(n)$ is calculated.

IV. ABSOLUTE REELS ANALYSIS

For the analysis of the REELS spectra in absolute units, a measured REELS spectrum $J(E)$ was corrected for the analyzer transmission function and normalized by the primary beam current. The transmission function of the CMA used in the present study was that estimated from a measurement of the transmission of light.¹⁰ These procedures provide units of the intensity of the REELS spectra to be (eV electron)⁻¹ (absolute units). The energy distribution of primary electrons $F(E)$ was deduced from the elastic peak of the REELS spectrum for low electron energies where the CMA energy resolution was sufficient. Using these $F(E)$ and $J(E)$ with the first equation of Eq. (16), the response function $R(\Delta E)$ describing the energy-loss probability distribution per incident electron was obtained.

In order to deduce IMFP λ_b , SEP P_s^{in} , and DSEP $K_s^{\text{in}}(\Delta E)$ from the experimentally obtained $R(\Delta E)$, the right-hand side of Eq. (17) must be solved using Eqs. (18)–(28). In the present analysis, IMFP λ_b , SEP P_s^{in} , and DSEP $K_s^{\text{in}}(\Delta E)$ were self-consistently determined. We first calculated the normalized DIMFP [Eq. (2)], $\lambda_b K_b(\Delta E)$, describing the energy loss distribution probability due to a single bulk excitation. The DIMFP $K_b(\Delta E)$ was calculated using dielectric response theory⁴⁵ with Penn's algorithm⁴⁶ based on the Ritchie-Howie algorithm⁴⁷ for the extension of the ω -dependent energy-loss function $\text{Im}[-1/\varepsilon(\omega)]$ to the momentum-energy loss ($q-\omega$) space.

$$K_b(\Delta E) = \frac{1}{2\pi a_0 E_0} \int_0^{E_p} \frac{d(\hbar\omega_0)}{\Delta E(\Delta E - \hbar\omega_0)} \hbar\omega_0 \times \text{Im} \left[\frac{-1}{\varepsilon(\omega_0)} \right] \Theta \left[\frac{\hbar^2}{2m} (2k\bar{q} - \bar{q}^2) - \Delta E \right]. \quad (29)$$

Here, a_0 is the Bohr radius, and $\Theta(x)$ is the step function representing the laws of momentum and energy conservation. The energy-loss function was calculated from optical data.⁴⁸ $\hbar\bar{q}$ is the momentum transfer satisfying the following dispersion relation:

$$\Delta E = \hbar\omega_0 + \hbar^2 \bar{q}^2 / 2m. \quad (30)$$

The normalized DIMFP $\lambda_b K_b(\Delta E)$ was then obtained by multiplying the DIMFP $K_b(\Delta E)$ [Eq. (29)] by the IMFP λ_b , which is a normalization factor obtained by integration of the DIMFP over energy loss [Eq. (2)]. Hereafter, the IMFP calculated from optical data is referred to as the optical IMFP

λ_{opt} . Note that the normalized DIMFP $\lambda_b K_b(\Delta E)$ is independent of λ_b .

α_m representing the probability that signal electrons experience m -fold bulk excitations is calculated as follows. Under the assumption that bulk excitations obey the Poisson stochastic process, α_m can be calculated from the path-length distribution $d\eta/dx$ for a primary electron and the IMFP λ_b using

$$\alpha_m = \int_0^\infty \frac{d\eta}{dx} \frac{1}{m!} \left(\frac{x}{\lambda_b}\right)^m \exp\left(-\frac{x}{\lambda_b}\right) dx, \quad (31)$$

where x is the path length. The path-length distribution $d\eta/dx$ is obtained by a Monte Carlo (MC) simulation, in which electron trajectories are traced by taking into account only elastic scattering. The (differential) elastic-scattering cross section is calculated using Mott cross sections calculated with the partial-wave expansion method using the Thomas-Fermi-Dirac potential.⁴⁹⁻⁵¹ Details of the MC simulations are described elsewhere.¹⁰

In the present analysis, α_m is first obtained from Eq. (31) using the optical IMFP and the path-length distribution from the MC simulation. This value of α_0 and the experimental elastic-peak intensity $[R(\Delta E=0)]_{m=0, l=0} = r(0)$ provides SEPs, P_s^{in} and P_s^{out} , using Eq. (17) with Eqs. (8) and (9). Then, $P_s^{\text{total}, l}$ is calculated from P_s^{in} using Eq. (14). θ_{out} is set at 42.3° as the average value of the detection angle for the CMA. Thus deconvolution of the response function $R(\Delta E)$ according to Eq. (17) using the normalized DIMFP $\lambda_b K_b(\Delta E)$ and values of α_m and $P_s^{\text{total}, l}$ enables the DSEP $K_s^{\text{in}}(\Delta E)$ to be obtained with the use of Eqs. (20), (27), and (28). In the present study, inelastic-scattering events satisfying $m+l \leq k=10$ were taken into account, which is sufficient for the analysis of a REELS spectrum over the energy region from the elastic peak to an energy loss of ~ 100 eV. The SEP P_s^{in} deduced from the elastic peak and the DSEP $K_s^{\text{in}}(\Delta E)$ deduced from the energy-loss spectrum obtained at this stage of the analysis does not satisfy the physically defined Eq. (4). In the next step of the analysis, the value of the IMFP is modified, and the SEP and DSEP are recalculated as described above. Modification of the IMFP and deducing the SEP and DSEP are iterated until the SEP and DSEP satisfy Eq. (4). Finally, the IMFP, SEP, and DSEP which satisfy all the above equations are self-consistently determined.

Note that the present procedure is possible only when the experimental spectra are measured in absolute units, and all the analysis were performed in absolute units. Most of the experimental IMFP determinations have been performed by analyzing only the elastic-peak intensity. In contrast, the present approach takes into account not only the elastic-peak intensity but also the energy-loss spectrum appearing on the lower energy side of the elastic peak. In addition, the present analysis does not require any reference materials, and the SEP and DSEP are also deduced from the absolute REELS spectrum simultaneously with IMFPs. Consequently, the present method enables a more physically consistent determination of IMFPs and SEPs.

It should be noted that the similar procedure to determine the SEP and DSEP from REELS spectra has been reported

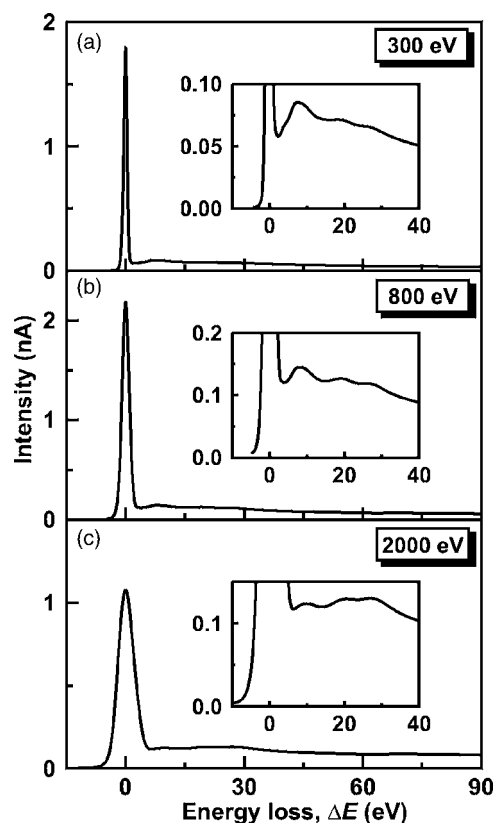


FIG. 1. REELS spectra from the Ni surface at the primary energies of (a) 300, (b) 800, and (c) 2000 eV. Insets show the spectra near the elastic peak on an enlarged scale.

and intensively studied.^{25,27,34-36} This previously reported procedure makes it possible to determine the SEP and DSEP and has been revealed to be effective in determining those physical parameters. However, as mentioned in Ref. 25, the proposed procedure requires the value of the IMFP to be known for calculating partial intensities for bulk excitations, though the derived SEP may not be affected significantly by the value of the IMFP.²⁵ In contrast, the present approach can be performed in absolute units, where units of the intensity of a spectrum is $(\text{eV electron})^{-1}$, throughout the analysis. The value of the IMFP is not an input parameter in the present analysis, and the IMFP is a parameter to be determined simultaneously with SEP and DSEP in absolute units from a REELS spectrum. Note that a procedure is described that allows one to find the DIMFP and the DSEP from two REELS spectra using the elastic cross section and an estimate for the IMFP (accurate to about 30%) as input parameters in Ref. 44.

V. RESULTS AND DISCUSSION

A. Deconvolution of response function

Figure 1 shows REELS spectra measured for Ni at primary energies of (a) 300, (b) 800, and (c) 2000 eV. The energy-loss structure near the elastic peak shown in the insets reveals that energy-loss peaks appearing at ΔE of ~ 7.5 and ~ 27.5 eV increased and decreased, respectively, as the

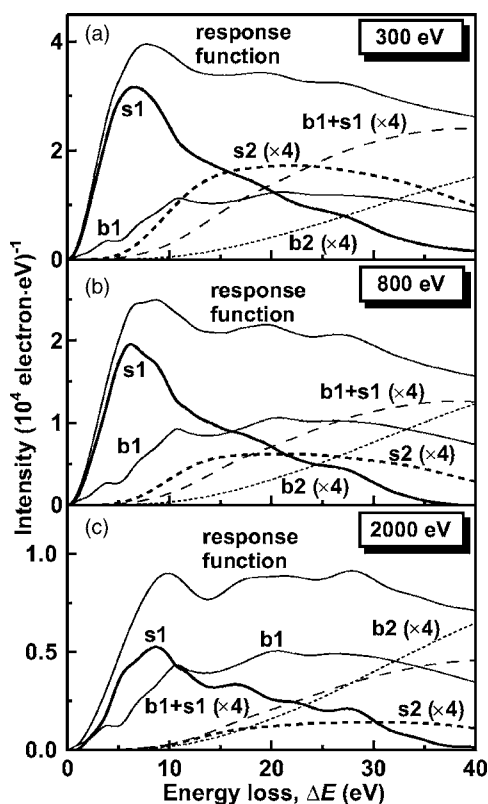


FIG. 2. Response functions of REELS spectra and their deconvolutions into components relevant to m -fold bulk and l -fold surface excitations at primary energies of (a) 300, (b) 800, and (c) 2000 eV. The components satisfying $m+l \leq 2$ are shown. Thick solid line: single surface excitation (s1; $m=0$ and $l=1$). Thin solid line: single bulk excitation (b1; $m=1$ and $l=0$). Thick dotted line: twofold surface excitation (s2; $m=0$ and $l=2$). Thin dotted line: twofold bulk excitation (b2; $m=2$ and $l=0$). Broken line: single surface and single bulk excitations ($b1+s1$; $m=1$ and $l=1$). The components corresponding to $m+l=2$ are multiplied by a factor of 4.

primary energy decreased. These peaks are attributed to surface and bulk excitations, respectively, since the contribution of surface excitations is significant for the lowest primary energy.

In the present analysis, the REELS spectrum $J(E)$ was deconvoluted into the source function $F(E)$ and the response function $R(\Delta E)$ according to Eq. (16). Each response function was further deconvoluted into each component representing the energy-loss probability due to m -fold bulk and l -fold surface excitations. It is of interest to investigate the relative contributions of surface and bulk excitations to the energy-loss spectrum. Figure 2 shows the resulting response functions and their deconvolution into each energy-loss component for primary energies of (a) 300, (b) 800, and (c) 2000 eV. Since the energy-loss spectrum close to the elastic peak is dominated by the lower-order components, only the components corresponding to $(m+l) \leq 2$ were plotted. It is clear that the ratio of the contribution of the component due to single bulk excitation (b1) to that due to single surface excitation (s1) strongly depends on primary energy. The energy-loss processes by surface excitations are more domi-

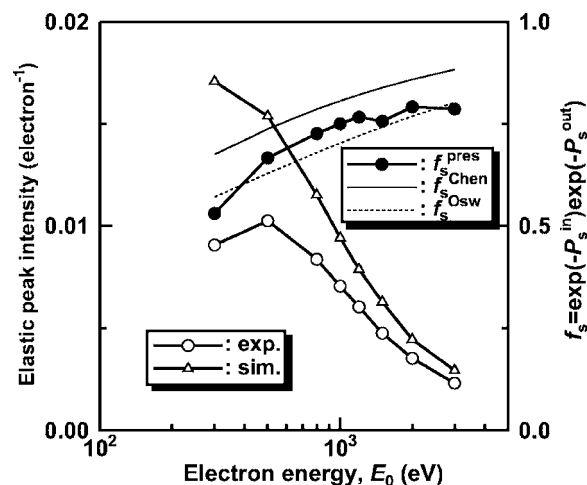


FIG. 3. Simulated (open triangles) and experimental (open circles) elastic-peak intensities and the surface excitation correction factor f_s (solid circles) as functions of primary electron energy. The simulated elastic-peak intensity was calculated with Eq. (31) for $m=0$ using the path-length distributions obtained from MC simulations. The surface excitation correction factor was calculated as the ratio of the experimental elastic-peak intensity to the simulated value (Ref. 8). The f_s estimated using Oswald (Ref. 52) and Chen (Ref. 53) formulas for SEP are also shown.

nant for low-energy electrons for the energy loss region near the elastic peak. It is also found that most of the energy-loss spectra in the region of $\Delta E=0-40$ eV, which is important for background subtraction in quantitative analysis using surface electron spectroscopy, consists of the lower order components with $m+l \leq 2$.

B. Surface excitation parameter

Signal electrons losing kinetic energy by surface excitation form the energy-loss structure observed in Fig. 2 with $l > 0$. In addition, surface excitations result in a decrease in the elastic-peak intensity. Figure 3 depicts the change in the elastic-peak intensity as a function of primary energy. The simulated elastic-peak intensity $I_{\text{sim}} = \alpha_0$, in which the decrease of the elastic-peak intensity due to bulk excitations was taken into consideration and that due to surface excitations was neglected, was calculated with Eq. (31) for $m=0$ using the path-length distribution, $d\eta/dx$, obtained by MC simulation (see Fig. 11). It is clear that the simulated intensity, I_{sim} , in which surface excitation is neglected, is larger than the experimental value, I_{exp} . The discrepancy between the simulated and experimental results is larger for lower primary energies. For a more quantitative comparison, the surface excitation correction factor f_s defined as¹⁰

$$f_s = \exp(-P_s^{\text{in}}) \exp(-P_s^{\text{out}}) = I_{\text{exp}} / I_{\text{sim}} \quad (32)$$

is also plotted in Fig. 3. For a comparison, the f_s estimated using Oswald⁵² and Chen⁵³ formulas for SEP are also shown. The present f_s is found to agree with that calculated using Oswald formula. Even when the electron energy is greater than 1000 eV, the peak intensity is decreased by $\sim 20\%$ due to surface excitation. The decrease of peak intensity is most

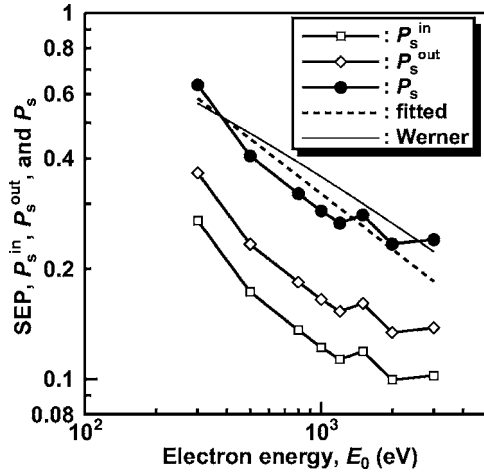


FIG. 4. Surface excitation parameters for incoming (P_s^{in} , open rectangles) and outgoing (P_s^{out} , open diamonds) electrons. P_s (solid circles) is the total SEP obtained as the sum of the SEPs for incoming and outgoing electrons. The dotted curve is that obtained by fitting the Chen equation [Eq. (34)] (Ref. 43) to the present results. The SEPs calculated using the equation reported by Werner *et al.* for Ni (Ref. 27) is also shown.

significant for the lower electron energies, and the decrease reaches $\sim 50\%$ at 300 eV. These findings suggest that surface excitation plays an important role in quantitative analysis in addition to bulk excitations, which also reduces the peak intensity, because of not only the significant decrease of the peak intensity but also the strong dependence of the contribution of surface excitation on the electron energy.

Figure 4 shows plots of the SEPs for incoming and outgoing electrons, P_s^{in} and P_s^{out} , and the total SEP defined as

$$P_s = P_s^{\text{in}} + P_s^{\text{out}} = [1 + \Theta(\theta_{\text{in}}, \theta_{\text{out}})] P_s^{\text{in}}. \quad (33)$$

P_s represents the average number of surface excitations experienced by a primary electron during its transport in the solid. The SEPs decrease as the electron energy increases as is usually observed. The SEP for 3 keV electrons is ~ 0.2 and increases to ~ 0.6 for 300 eV electrons, indicating that the average number of surface excitation events undergone by 300 eV electrons is three times larger than that experienced by 3 keV electrons. There is thus a significant decrease of the elastic-peak intensity at low primary energies, as confirmed by Fig. 3. The present SEPs can be fitted with the simple Chen equation,⁴³

$$P_s = \frac{a}{\sqrt{E}} \left(\frac{1}{\cos \theta_{\text{in}}} + \frac{1}{\cos \theta_{\text{out}}} \right). \quad (34)$$

This fit gives $a=4.3$ ($\text{eV}^{1/2}$) with an rms deviation of 0.038, as plotted by the dashed line in Fig. 4. For a comparison, the SEPs calculated using the equation recently reported by Werner *et al.* for Ni,²⁷ which is determined by the deconvolution of the REELS spectrum, is also shown in Fig. 4. A comparison revealed that the present SEPs agree reasonably well with those calculated by the Werner's predictive equation, indicating that the deconvolution of a REELS spectrum

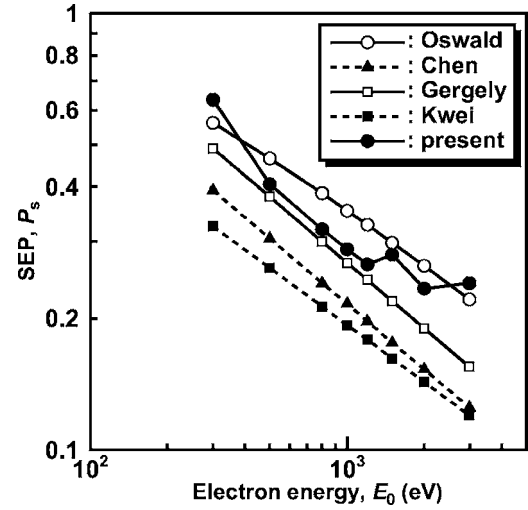


FIG. 5. Surface excitation parameters determined in the present study (solid circles) and those calculated from the predictive equations: Oswald's equation (Ref. 52) (open circles), Chen's equation for a free electron metal (Ref. 53) (closed triangle), Chen's equation (Ref. 43) with the material parameter $a=3.61$ for Ni proposed by Gergely *et al.* (Ref. 15) (open squares), and Kwei's equation (Ref. 54) (closed squares). For Kwei's equation, the angular dependence of the SEP was assumed to obey the cosine law.

(REELS analysis)^{24–30} is one of the most powerful approaches for determining SEPs.

The present SEPs are now compared in Fig. 5 with those calculated from several predictive equations, i.e., Oswald's equation,⁵² Chen's equation for a free electron metal,⁵³ Chen's equation⁴³ with the parameter $a=3.61$ proposed for Ni by Gergely *et al.*,¹⁵ and Kwei's equation,⁵⁴ as shown in Fig. 5. For the calculation of the SEP using Kwei's equation, the angular dependence, which was not reported in the paper, was assumed to obey the cosine law. Figure 5 shows that the present SEPs are close to those given by Oswald's equation⁵² at the low (300–500 eV) and high (1000–3000 eV) electron energies, and to those calculated using Chen's equation⁴³ with $a=3.61$ (Ref. 15) in the intermediate-energy region (500–1000 eV).

C. Inelastic mean-free path

The present absolute analysis of REELS spectra enables IMFPs to be determined simultaneously with the SEPs. Figure 6 shows plots of the IMFPs determined from the present REELS analysis, λ_{pres} , with those calculated using the TPP-2M predictive equation,⁴ λ_{TPP} , and the optical IMFPs calculated with Eqs. (2), (29), and (30), using optical data,^{45–48} λ_{opt} . It is found that λ_{pres} at the low electron energies agrees with λ_{TPP} and is smaller than λ_{TPP} at higher energies. For a better comparison, the percentage difference of λ_{pres} from λ_{TPP} , defined as⁹

$$\Delta\lambda_{\text{TPP}} = (\lambda_{\text{pres}} - \lambda_{\text{TPP}}) \times 100/\lambda_{\text{TPP}}, \quad (35)$$

is also plotted in Fig. 6 as a function of electron energy. The similar percentage difference, $\Delta\lambda_{\text{opt}}$, for λ_{opt} is also plotted in Fig. 6. Both $\Delta\lambda_{\text{TPP}}$ and $\Delta\lambda_{\text{opt}}$ are slightly positive at low

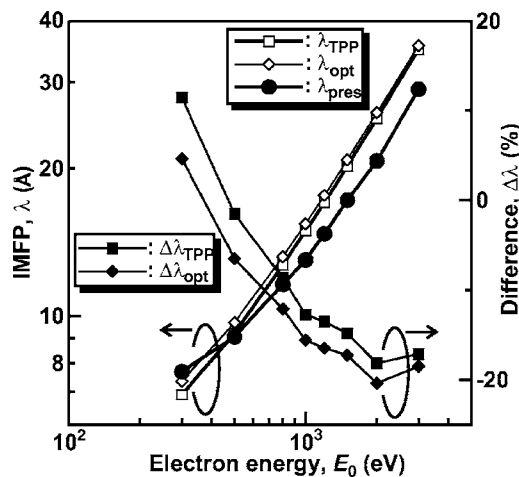


FIG. 6. IMFPs determined in the present study, λ_{pres} , and those calculated from the TPP-2M predictive equation (Ref. 4), λ_{TPP} , and the optical IMFP, λ_{opt} , calculated using optical data (Refs. 45–48). $\Delta\lambda_{\text{TPP}}$ and $\Delta\lambda_{\text{opt}}$ are the percentage differences of λ_{pres} from λ_{TPP} and λ_{opt} defined by Eq. (35).

energies and negative for high energies. The root-mean-square difference rms defined as⁹

$$\text{rms} = \sqrt{\frac{1}{r} \sum_{j=1}^r (\lambda_{\text{pres}} - \lambda_{\text{TPP}})^2} \quad (36)$$

was calculated to be 3.1 Å, where r is the number of IMFP data values. This rms value indicates that the IMFPs deduced from the present absolute analysis agree reasonably well with the theoretical predictions, confirming that the present approach is effective for the experimental determination of IMFPs.

Since the advantage of the present analysis is that the IMFP and SEP are simultaneously determined, the effects of the IMFP on the derivation of the SEP were investigated. For this, the SEPs were deduced from the REELS spectra by two conventional approaches, i.e., EPES analysis^{10,14,15,22,23} and REELS analysis.^{24–30} Since both approaches require the IMFP as input data, λ_{TPP} was employed for the IMFP, and the SEPs deduced by those two approaches were compared with values from the present approach. The SEPs deduced by the EPES analysis were determined from the experimental elastic-peak intensity, I_{exp} , and from the simulated value, I_{sim} , using Eq. (32). The simulated intensity, $I_{\text{sim}} = \alpha_0$, was calculated from the path-length distribution, $d\eta/dx$, obtained by MC simulation (see Fig. 11) using Eq. (31) and λ_{TPP} . The SEPs deduced from the REELS analysis were determined as the ratio of the area of the component due to single-surface excitation ($m=0$ and $l=1$) to the elastic-peak intensity ($m=0$, $l=0$, and $\Delta E=0$) in the response function, with each determined using λ_{TPP} , [see Eq. (17)], i.e.,

$$P_s = \frac{\int R(\Delta E)_{m=0,l=1} d(\Delta E)}{R(\Delta E=0)_{m=0,l=0}} = \frac{\alpha_0 (P_s^{\text{in}} + P_s^{\text{out}}) \exp[-(P_s^{\text{in}} + P_s^{\text{out}})]}{\alpha_0 \exp[-(P_s^{\text{in}} + P_s^{\text{out}})]}. \quad (37)$$

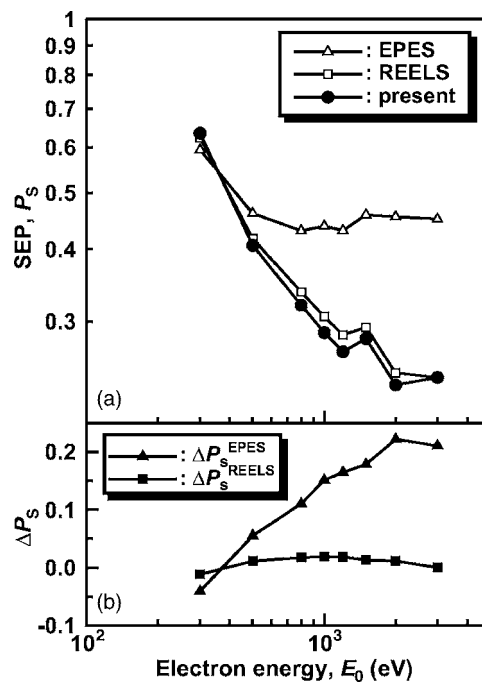


FIG. 7. (a) Total SEPs deduced by the present analysis (closed circles) and those determined by the EPES analysis (open triangles) and the REELS analysis (open squares) using λ_{TPP} as input data. (b) The differences in the SEPs determined by the present analysis from those obtained by the EPES analysis, ΔP_s^{EPES} , and by the REELS analysis, $\Delta P_s^{\text{REELS}}$.

Those SEPs determined by the EPES (open triangles) and REELS (open rectangles) analyses using λ_{TPP} are shown with the SEP obtained by the present analysis (solid circles) in Fig. 7(a). The difference between the SEP determined by the EPES analysis with λ_{TPP} and that determined by the present analysis, ΔP_s^{EPES} , and the difference between the SEP determined by the REELS analysis with λ_{TPP} and that determined by the present analysis, $\Delta P_s^{\text{REELS}}$, are plotted in Fig. 7(b). It is found that ΔP_s^{EPES} is large, particularly for higher electron energies. This is because the percentage difference between λ_{TPP} and λ_{pres} shown in Fig. 6 is larger at higher electron energies. In contrast, $\Delta P_s^{\text{REELS}}$ is small compared with ΔP_s^{EPES} , in spite of the same influence of λ_{TPP} in the REELS analysis as that in the EPES analysis. This is attributed to the procedure itself. Since the effects of λ_{TPP} describing bulk excitations are mainly introduced through α_0 in Eq. (37), the effects are almost canceled out between the numerator and denominator in Eq. (37). These findings revealed that, although the EPES analysis is one of the most powerful approaches to experimentally determining the SEP, care is required since the deduced SEP is sensitive to the value of the IMFP. In contrast, the SEP determined by the REELS analysis is rather insensitive to the IMFP used as input data. It should be noted that the EPES analysis described above was performed in absolute units without reference materials, resulting in significant effects of λ_{TPP} on the deduced SEPs. Note that the present analysis is a unique approach to determining both the IMFP and SEP simultaneously in absolute units from one REELS spectrum.

TABLE I. Parameters in the model dielectric function of Eq. (42) for Ni. $\epsilon_b=0.94$.

A_i (eV ²)	γ_i (eV)	ω_i (eV)	A_i (eV ²)	γ_i (eV)	ω_i (eV)
48.20	0.41	0.00	313.48	26.54	29.95
48.32	1.93	1.50	89.38	16.84	52.42
7.86	1.57	3.01	28.05	3.98	67.18
50.30	2.28	4.63	61.29	11.78	73.21
35.05	3.92	7.98	420.30	42.01	85.16
185.28	11.37	15.10	662.02	128.58	149.54
8.94	4.12	24.20			

D. Bulk and surface excitations

The shape of the DSEP describing the energy-loss distribution due to surface excitations is now compared with that predicted by the theory of Tung *et al.*⁵⁵ The equation for the DSEP in Tung's model is given in atomic units as

$$K_s^{\text{Tung}}(\omega) = K_s^+(\omega) + K_s^-(\omega), \quad (38)$$

and

$$K_s^\pm(\omega) = \frac{2}{\pi v^2 \cos \theta} \int_{k_-}^{k_+} \frac{|k'_s|}{k^3} \text{Im} \left[\frac{(\epsilon - 1)^2}{\epsilon(\epsilon + 1)} \right] dk, \quad (39)$$

where ω is the energy loss, v is the velocity of the electron, θ is the surface crossing direction, and

$$k'_s = \left[k^2 - \left(\frac{\omega}{v} + \frac{k^2}{2v} \right)^2 \right]^{1/2} \cos \theta \pm \left(\frac{\omega}{v} + \frac{k^2}{2v} \right) \sin \theta \quad (40)$$

and

$$k_\pm = \sqrt{2E_0} \pm \sqrt{2(E_0 - \omega)}. \quad (41)$$

For calculating the $K_s^{\text{Tung}}(\omega)$, the dielectric function $\epsilon(k, \omega) = \epsilon_1(k, \omega) + i\epsilon_2(k, \omega)$ was modeled by fitting a Drude-Lindhard type of expansion to optical data,⁵⁵

$$\epsilon_1(k, \omega) = \epsilon_b - \sum_i \frac{A_i [\omega^2 - (\omega_i + k^2/2)^2]}{[\omega^2 - (\omega_i + k^2/2)^2]^2 + \omega^2 \gamma_i^2}, \quad (42a)$$

$$\epsilon_2(k, \omega) = \sum_i \frac{A_i \gamma_i \omega}{[\omega^2 - (\omega_i + k^2/2)^2]^2 + \omega^2 \gamma_i^2}. \quad (42b)$$

In Table I, parameters in the model dielectric function obtained by a fit of Eq. (42), in the limit of $k \rightarrow 0$, to optical data for Ni (Ref. 48) are listed. The accuracy of the model dielectric function was confirmed by two sum rules, i.e., the oscillator strength rule and a limiting form of the Kramers-Kronig integral.^{2,48} Figure 8 shows a comparison of $\epsilon_1(0, \omega)$, $\epsilon_2(0, \omega)$, and $\text{Im}[-1/\epsilon(0, \omega)]$ for Ni calculated from optical data (broken lines) and those by Eq. (42) (solid lines). The fitted curves are in good agreement with those calculated from optical data.

Figures 9(a) and 9(b) show plots of DSEPs for incoming electrons from the present analysis and those calculated using Tung's model⁵⁵ [Eq. (38)]. For comparison, DIMFPs de-

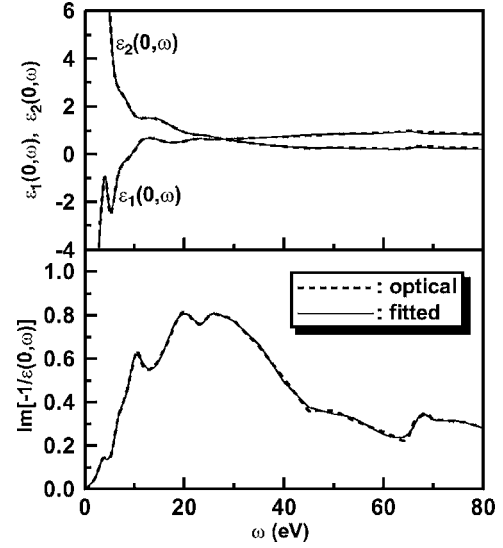


FIG. 8. A comparison of $\epsilon_1(0, \omega)$, $\epsilon_2(0, \omega)$, and $\text{Im}[-1/\epsilon(0, \omega)]$ for Ni calculated from optical data (Ref. 48) (broken lines) and those by Eq. (42) (solid lines).

termined in the present study, which satisfy Eq. (2) with λ_{pres} , are shown in Fig. 9(c). A comparison between the DSEP in Fig. 9(a) and DIMFP in Fig. 9(c) reveals that the energy loss processes in the low-energy loss region are domi-

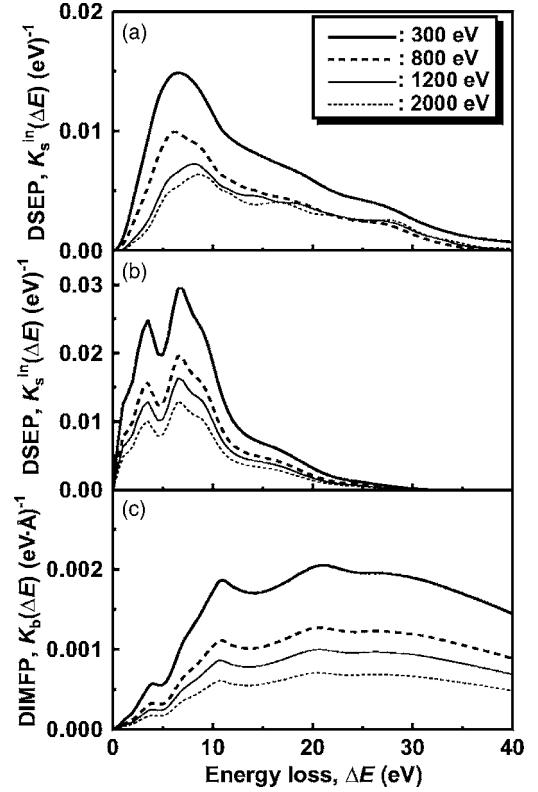


FIG. 9. (a) DSEPs for incoming electrons determined from the present analysis. (b) DSEPs calculated using Tung's model [Eq. (38)] (Ref. 55). (c) DIMFPs determined in the present study. The shape of the DIMFP is the same as that of the optical DIMFP and the intensity of the DIMFP satisfies Eq. (2) with λ_{pres} .

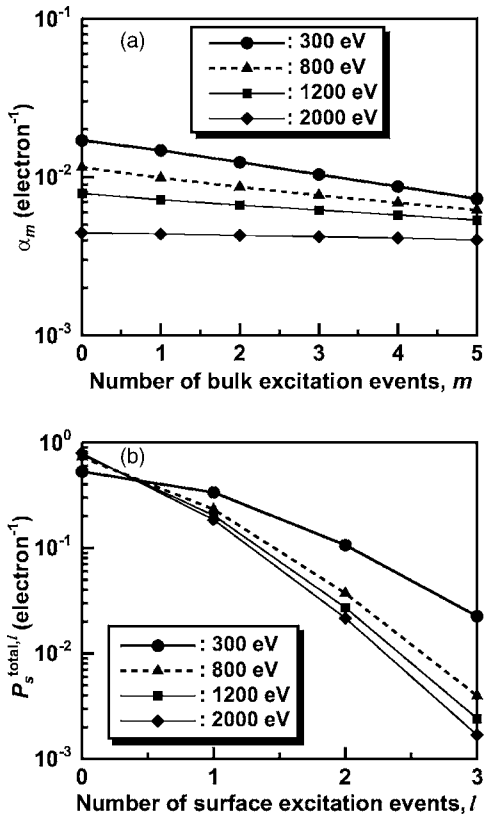


FIG. 10. (a) α_m and (b) $P_s^{\text{total},l}$ determined from the present REELS analysis.

nated by surface excitations. In bulk and surface excitations, the lower the electron energy is, the higher the energy loss probability is. A comparison between Figs. 9(a) and 9(b) reveals that the overall agreement between the present DSEP and theory is reasonable, particularly, the most probable energy loss by single surface excitation is found to be approximately 7.5 eV in both the present analysis and theory. However, discrepancies between the present DSEP and theory are found for energy losses larger than 15 eV. This might be attributed to the deficiencies in the optical data²⁷ used for calculating the normalized DIMFP for bulk excitation in the present deconvolution procedure and for parametrization of the model dielectric function for calculating the theoretical DSEP.

Figures 10(a) and 10(b) show α_m and $P_s^{\text{total},l}$, respectively, and indicate how multiple bulk and surface excitations contribute to the REELS spectra. In the case of bulk excitations, the number of electrons participating in the smaller number of bulk excitations is larger for lower-energy electrons. For higher electron energies, the probabilities of electrons participating in zero- to fivefold bulk excitations are almost the same and independent of the number of bulk excitations. This tendency can be easily understood from the path-length distribution $d\eta/dx$, calculated by MC simulation, shown in Fig. 11. The path-length distribution for 300 eV electrons has a peak at ~ 0.3 nm and increases with longer path length. As the energy increases, electrons penetrate deeper. The path-length distribution decreases, particularly for short path lengths, and becomes featureless. The almost constant path-

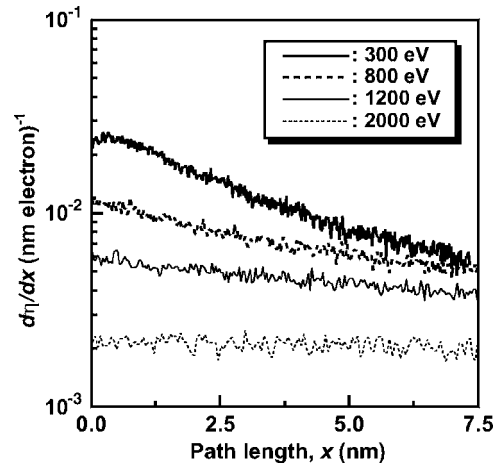


FIG. 11. Path-length distributions $d\eta/dx$ obtained by MC simulation.

length distribution in Fig. 11 provides the flat distribution of α_m in Fig. 10(a) for $E_0=2$ keV. With respect to surface excitations, the probability that electrons participate in l -fold events strongly depends on the number of surface excitation events l . Most electrons (50%–80%) undergo no surface excitations. The probability for $l \geq 3$ is below $\sim 1\%$. The sum of $P_s^{\text{total},0}$ and $P_s^{\text{total},1}$ is ~ 0.86 to ~ 0.96 for 300–3000 eV electrons, indicating that only zero or single surface excitations are dominant for medium-energy electrons.

Figure 12 shows plots of the probability $\alpha_m P_s^{\text{total},l}$ of electrons undergoing m -fold bulk and l -fold surface excitations,

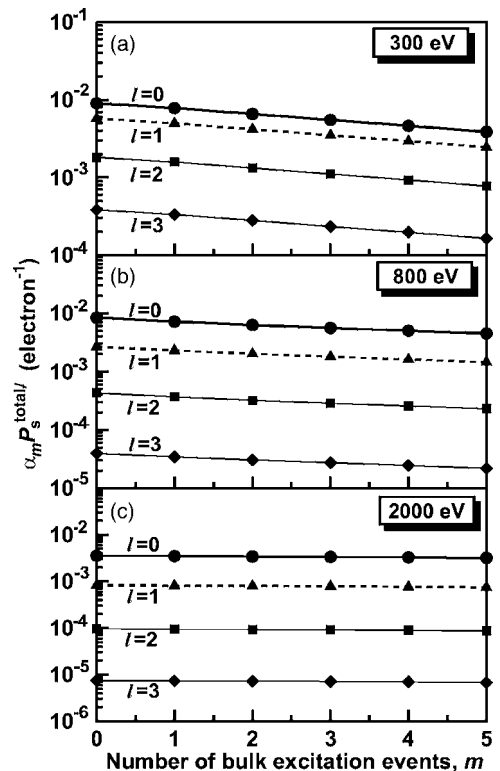


FIG. 12. Probabilities of electrons participating in m -fold bulk and l -fold surface excitation events during transport in Ni before being detected by the CMA.

which corresponds to the areas of the components relevant to m -fold bulk and l -fold surface excitations in the response function (see Fig. 2). It can be easily seen that the contribution of the single surface excitation ($l=1$) is $\sim 60\%$ of that of $l=0$ for 300 eV, and decreases to $\sim 20\%$ for 2000 eV. The contribution of twofold surface excitation events to the REELS spectrum is still $\sim 20\%$ for 300 eV, and decreases to only a few percent for 2000 eV. These results indicate that surface excitations play an important role for medium-energy electrons. The contribution of surface excitations strongly depends on the energy of signal electrons, suggesting that care concerning surface excitations is required for the improvement of the accuracy of quantification using surface electron spectroscopy.

VI. CONCLUSIONS

In the present paper, an analytical approach to deducing the SEP, DSEP, and IMFP in absolute units from a REELS spectrum was proposed and applied to the analysis of the REELS spectra for Ni. The obtained results are summarized as follows.

(1) The response function obtained by deconvolution of the REELS spectrum with the energy distribution of primary electrons was further deconvoluted self-consistently into components due to m -fold bulk and l -fold surface excitations. The lower the electron energy is, the larger the contribution of single surface excitations is. The energy-loss spectrum close to the elastic peak was dominated by electrons undergoing single bulk or surface excitations.

(2) The absolutely determined IMFPs showed good agreement with those obtained using the TPP-2M predictive equation and theory based on optical data. The rms difference between the present IMFPs and those calculated with the TPP-2M equations was 3.1 \AA .

(3) The effects of the IMFP on the determination of the SEP were investigated. The results revealed that the SEP determined by the REELS analysis is insensitive to the value of the IMFP used in the analysis.

(4) The Chen equation described SEPs from the present analysis. Comparison of the present SEPs with those calculated using several predictive equations revealed that our SEPs are close to those given by Oswald's equation at low (300–500 eV) and high (1000–2000 eV) electron energies, and to those calculated using Chen's equation with $a=3.61$,¹⁵ as proposed for Ni by Gergely *et al.* in the intermediate (500–1000 eV) energy region.

(5) The DSEP was also determined from the REELS analysis. The overall agreement between the preset DSEPs and those calculated using Tung's model is found to be reasonable.

Consequently, the present method for analyzing REELS spectra has a high potential for the experimental determination of the IMFP, SEP, and DSEP in absolute units. Further detailed study is under way and will be reported shortly.

ACKNOWLEDGMENT

The authors would like to thank S. Tanuma and H. Yoshikawa (NIMS, Japan) for helpful discussions.

*Corresponding author.

Electronic address: nagatomi@mls.eng.osaka-u.ac.jp

- ¹S. Tanuma, C. J. Powell, and D. R. Penn, *Surf. Interface Anal.* **17**, 911 (1991).
- ²S. Tanuma, C. J. Powell, and D. R. Penn, *Surf. Interface Anal.* **17**, 927 (1991).
- ³S. Tanuma, C. J. Powell, and D. R. Penn, *Surf. Interface Anal.* **20**, 77 (1993).
- ⁴S. Tanuma, C. J. Powell, and D. R. Penn, *Surf. Interface Anal.* **21**, 165 (1994).
- ⁵S. Tanuma, C. J. Powell, and D. R. Penn, *Surf. Interface Anal.* **25**, 25 (1997).
- ⁶S. Tanuma, C. J. Powell, and D. R. Penn, *Surf. Interface Anal.* **35**, 268 (2003).
- ⁷S. Tanuma, C. J. Powell, and D. R. Penn, *Surf. Interface Anal.* **36**, 1 (2004).
- ⁸G. Gergely, *Prog. Surf. Sci.* **71**, 31 (2002).
- ⁹C. J. Powell and A. Jablonski, *J. Phys. Chem. Ref. Data* **28**, 19 (1999).
- ¹⁰S. Tanuma, S. Ichimura, and K. Goto, *Surf. Interface Anal.* **30**, 212 (2000).
- ¹¹W. S. M. Werner, C. Tomastik, T. Cabela, G. Richter, and H. Störi, *Surf. Sci.* **470**, L123 (2000).
- ¹²W. S. M. Werner, C. Tomastik, T. Cabela, G. Richter, and H. Störi, *J. Electron Spectrosc. Relat. Phenom.* **113**, 127 (2001).
- ¹³M. Krawczyk, A. Jablonski, L. Zommer, J. Tóth, D. Varga, L. Kövér, G. Gergely, M. Menyhard, A. Sulyok, Zs. Bendek, B. Gruzza, and C. Robert, *Surf. Interface Anal.* **33**, 23 (2002).
- ¹⁴J. Zemek, P. Jiricek, B. Lesiak, and A. Jablonski, *Surf. Sci.* **531**, L335 (2003).
- ¹⁵G. Gergely, M. Menyhard, S. Gurban, J. Toth, and D. Varga, *Surf. Interface Anal.* **36**, 1098 (2004).
- ¹⁶Y. F. Chen and Y. T. Chen, *Phys. Rev. B* **53**, 4980 (1996).
- ¹⁷C. M. Kwei, C. Y. Wang, and C. J. Tung, *Surf. Interface Anal.* **26**, 682 (1998).
- ¹⁸T. Nagatomi, R. Shimizu, and R. H. Ritchie, *Surf. Sci.* **419**, 158 (1999).
- ¹⁹Z. J. Ding, H. M. Li, Q. R. Pu, Z. M. Zhang, and R. Shimizu, *Phys. Rev. B* **66**, 085411 (2002).
- ²⁰W. S. M. Werner, C. Eisenmenger-Sittner, J. Zemek, and P. Jiricek, *Phys. Rev. B* **67**, 155412 (2003).
- ²¹F. Yubero and S. Tougaard, *Phys. Rev. B* **71**, 045414 (2005).
- ²²G. Gergely, M. Menyhard, S. Gurban, J. Toth, and D. Varga, *Surf. Interface Anal.* **36**, 1098 (2004).
- ²³S. Gurban, G. Gergely, J. Toth, D. Varga, A. Jablonski, and M. Menyhard, *Surf. Interface Anal.* **38**, 624 (2006).
- ²⁴W. S. M. Werner, W. Smekal, C. Tomastik, and H. Störi, *Surf. Sci.* **486**, L461 (2001).
- ²⁵W. S. M. Werner, *Surf. Sci.* **526**, L159 (2003).
- ²⁶W. S. M. Werner, *Surf. Interface Anal.* **35**, 347 (2003).

- ²⁷W. S. M. Werner, L. Köver, S. Egri, J. Tóth, and D. Varga, *Surf. Sci.* **585**, 85 (2005).
- ²⁸G. Gergely, M. Menyhard, S. Gurban, A. Sulyok, J. Toth, D. Varga, and S. Tougaard, *Solid State Ionics* **141-142**, 47 (2001).
- ²⁹G. Gergely, M. Menyhard, S. Gurban, A. Sulyok, J. Toth, D. Varga, and S. Tougaard, *Surf. Interface Anal.* **33**, 410 (2002).
- ³⁰S. Gurban, G. Gergely, M. Menyhard, J. Adam, A. Adamik, Cs. Daroczi, J. Toth, D. Varga, A. Csik, and S. Tougaard, *Surf. Interface Anal.* **34**, 206 (2002).
- ³¹T. Nagatomi and K. Goto, *Appl. Phys. Lett.* **87**, 224107 (2005).
- ³²L. Landau, *J. Phys. (Moscow)* **8**, 201 (1944).
- ³³K. Goto, N. Sakakibara, and Y. Sakai, *Microbeam Anal.* **2**, 123 (1993).
- ³⁴W. S. M. Werner, *Surf. Interface Anal.* **35**, 347 (2003).
- ³⁵W. S. M. Werner and P. Schattschneider, *J. Electron Spectrosc. Relat. Phenom.* **143**, 65 (2005).
- ³⁶W. S. M. Werner, in *Surface Analysis by Auger and X-Ray Photoelectron Spectroscopy*, edited by D. Briggs and J. T. Grant (IM Publications, Chichester, UK, 2003), Chap. 10.
- ³⁷H. Yoshikawa, Y. Irokawa, and R. Shimizu, *J. Vac. Sci. Technol. A* **13**, 1984 (1995).
- ³⁸T. Nagatomi, T. Kawano, and R. Shimizu, *J. Appl. Phys.* **83**, 8016 (1998).
- ³⁹T. Nagatomi, R. Shimizu, and R. H. Ritchie, *J. Appl. Phys.* **85**, 4231 (1999).
- ⁴⁰W. S. M. Werner, *Phys. Rev. B* **55**, 14925 (1997).
- ⁴¹Y. F. Chen, *Surf. Sci.* **345**, 213 (1996).
- ⁴²Y. F. Chen and C. M. Kwei, *Surf. Sci.* **364**, 131 (1996).
- ⁴³Y. F. Chen, *Surf. Sci.* **519**, 115 (2002).
- ⁴⁴W. S. M. Werner, *Phys. Rev. B* **74**, 075421 (2006).
- ⁴⁵D. Pines, *Elementary Excitations in Solids* (W.A. Benjamin, New York, 1964).
- ⁴⁶D. R. Penn, *Phys. Rev. B* **35**, 482 (1987).
- ⁴⁷R. H. Ritchie and A. Howie, *Philos. Mag.* **36**, 463 (1977).
- ⁴⁸E. D. Palik, *Handbook of Optical Constants of Solids* (Academic, New York, 1985).
- ⁴⁹N. F. Mott and H. S. W. Massey, *The Theory of Atomic Collisions*, 6th ed. (Oxford, London, 1965).
- ⁵⁰Y. Yamazaki, Ph.D. thesis, Osaka University, 1977.
- ⁵¹S. Ichimura and R. Shimizu, *Surf. Sci.* **112**, 386 (1981).
- ⁵²R. Oswald, Ph.D. thesis, Eberhard-Karls-Universität, Tübingen, 1992.
- ⁵³Y. F. Chen, *Surf. Sci.* **380**, 199 (1997).
- ⁵⁴C. M. Kwei, C. Y. Wang, and C. J. Tung, *Surf. Interface Anal.* **26**, 682 (1998).
- ⁵⁵C. J. Tung, Y. F. Chen, C. M. Kwei, and T. L. Chou, *Phys. Rev. B* **49**, 16684 (1994).